Respiratory Motion Modeling in Small Animal PET Using GATE

S. Branco[1], S. Jan[2] and P. Almeida[1]

[1]Universidade de Lisboa, Faculdade de Ciências, Instituto de Biofísica e Engenharia Biomédica, Lisboa, Portugal
[2]CEA/DSV/I[2]BM, Service Hospitalier Frédéric Joliot, Orsay, France

***Abstract*–Respiratory motion is one source of degradation in PET images. Respiration leads to reduced contrast and quantitative accuracy in terms of recovered activity concentration and functional volumes, as a result of the associated image blurring. Consequently, the motion of lungs hindering the localization, detection, and the quantification of tracer uptake in lung lesions.**

Our long term goal is to study the impact of respiratory motion and evaluate the degradation on lesion detection in PET images. For that purpose, we used Monte Carlo simulations to produce realistic simulated data for the FDG radiotracer using the dynamic respiratory feature available in the 4D Mouse Whole-Body (MOBY) phantom including a lung lesion model.

I. INTRODUCTION

It is known that the localization and detection of thoracic and abdominal lesions in PET imaging is often perturbed due to the displacement of the organs during normal breathing. The respiratory motion compromise image quality and quantification in PET, and affect clinical diagnosis. To compensate respiratory motion, simulation using software packages may provide a valuable tool for the assessment of respiratory motion detection and correction.

In order to contribute for the full understanding of this problem, we used the Geant4 Application for Tomographic Emission (GATE) Monte Carlo platform [1] to model the microPET® FOCUS 220 system and the MOBY phantom [4] to produce realistic simulated mouse scans. GATE is a toolkit for PET and SPECT Monte Carlo simulation in nuclear medicine. MOBY was developed to provide a realistic and flexible model of the mouse anatomy and physiology to be used in molecular imaging research.

The aim of this work is to produce realistic simulated data for the *2-Deoxy-[^{18}F]fluoro-D-glucose* (FDG) radiotracer using the dynamic respiratory feature available in the MOBY phantom including a lung lesion model, to evaluate the effect of the respiratory motion on image quantification. These simulated data will be useful to evaluate the degradation on lesion detection due to normal breathing in whole-body mouse PET imaging, and hopefully shed some additional light on dealing with this problem in human exams.

II. MATERIAL AND METHODS

A. *The GATE platform*

GATE is a generic Monte Carlo simulation platform dedicated to nuclear medicine, based on Geant4 libraries, a well-established code for the simulation of radiation transport. GATE encapsulates the Geant4 libraries to achieve a modular, versatile and scripted simulation toolkit adapted to emission and transmission tomography. The use of GATE facilitates the description of different components necessary for the accurate modelling of a PET or a SPECT system, starting from the geometry up to the creation of a processing chain for the detected events. It allows describing time-dependent phenomena such as detector or patient movements, source decay kinetics and dead time for coincidence acquisitions including delay coincidences measurement.

1) Modelling the microPET® FOCUS 220

We modelled the microPET® FOCUS 220 system within the GATE platform. The system is suitable for acquiring high resolution images of small animal as rodents (mice and rats) and primates (macaque and small baboon). Its axial Field of View (FOV) is 7.6 cm and has a diameter of 26.0 cm. The FOCUS system has a volume resolution of 2.5 μL and an absolute sensitivity of 3.4 %, both measured at the center of the FOV [2]. The complete validation results of the microPET® FOCUS 220 simulation system using GATE can be found in [3].

2) The MOBY phantom description within GATE

The MOBY mouse phantom combines the realism of a voxelized phantom, with the flexibility of a mathematical phantom, based on non-uniform rational B-splines (NURBS). We applied a resampling on the default MOBY matrix to reduce the voxel number to 40×40×124 voxels with a voxel unit size of 0.5×0.5×0.5 mm^3. This allowed to significantly reduce the computational time resulting from the particle tracking inside the simulated volume and took into account the spatial resolution of the scanner.

The MOBY phantom includes 4D models of the mouse's cardiac and respiratory motions. The MOBY respiratory motion was set up to be dependent on two time varying parameters: the change in the height of the diaphragm and the amount of chest expansion. We manipulated these parameters to produce a "stress breathing" condition, in order to reproduce the respiratory motion of a mouse during a typical PET examination: the diaphragm height was set to 6.0 mm and the expansion of the chest was set to 4.2 mm.

A spherical lung lesion was implemented in the middle region of the left lung and its motion modelled as a function of the non normal tidal breathing condition. The motion of a specific spot of

978-1-4244-2715-4/08/$25.00 ©2008 IEEE

the lung is modelled as a two-way motion between two points in space, with same cycle of the diaphragm movement. For a respiratory cycle with a typical period of 0.37 s, the diaphragm motion can be decided by:

$$\Delta_{diaphr}(t) = \begin{cases} 0.5mm\cos\left(\frac{\pi}{0.16}t\right) + 0.5 & 0 \le t \le 0.16s \\ 0.5mm\cos\left(\frac{\pi}{0.24}(0.4-t)\right) + 0.5 & 0.16s \le t \le 0.4s \end{cases} \quad (1)$$

Based on (1), a set of 10 temporal frames (gates) of 0.037 s was generated over a complete respiratory cycle of 0.37 s in addition to a non-gated data set.

The parameter curves for both respiratory and lesion motion it's shown in Fig. 1. The MOBY phantom is illustrated in Fig. 2..

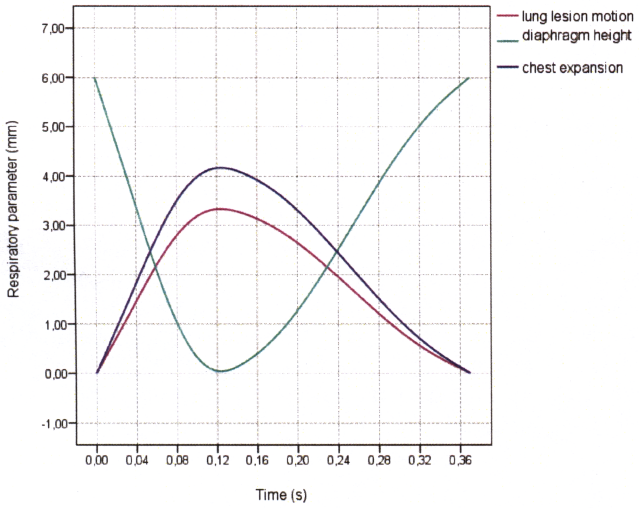

Fig. 1. Parameter curves for the "stress" breathing condition in the MOBY phantom.

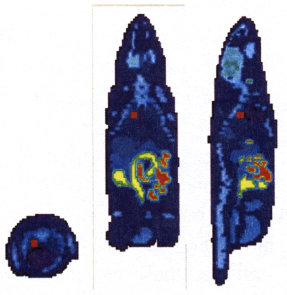

Fig. 2. Slices of the emission map of the MOBY phantom including a spherical lesion in middle region of the left lung.

B. *Simulation and reconstruction set-up*

In order to investigate the effect of the respiratory motion on 3D and 4D microPET images, a set of static (non-gated MOBY data set) and dynamic (gated MOBY data set) FDG simulations, for the last time frame, were performed considering different lesion diameter (0.75 mm, 1.0 mm, 1.25 mm, 1.5 mm and 2.0 mm) and different activity uptakes of FDG (0.03 μCi, 0.05 μCi, 0.08 μCi, 1.08 μCi and 1.35 μCi).

The gated and non-gated MOBY emission maps are integrated into GATE as voxelized sources to assign the activity to different anatomical structures, in order to obtain static and dynamic emission data sets.

The activity distribution in all of the other organs was defined according to the last acquisition time frame for an FDG exam (determined with a typical mouse FDG-PET exam). The concentration activity of the last frame (900 s of acquisition time) corresponds to a 131 μCi.

The FDG biodistribution was defined by the Time Activity Curves (TACs) obtained from real whole-body mouse PET exams. The activity distribution, within the MOBY phantom, was set according to the activity distribution assigned to the different whole body structures for the FDG radiotracer. In all simulation protocols physical effects like positron range, gamma accolinearity and tissue attenuation were not taken into account in order to obtain the "best case scenario", which could be used as defining the optimal results that we could obtain with a dedicated scanner and a specific radiotracer. Simulated data were rebinned with the Fourier Rebinning algorithm (FORE) and reconstructed using the OSEM2D method (16 subsets and 4 iterations).

C. *Data Analysis*

The spatial resolution was measured by the full width at the half maximum (FWHM) and full width at the tenth maximum (FWTM).The FWHMs of reconstructed lesion images were determined along the direction of lesion movement due to respiratory motion.

The image statistics were evaluated by calculating the signal-to-noise ratio (SNR) and contrast-to-noise ratio (CNR). The SNR is defined as the ratio of the average activity concentration measured in the target to the standard deviation. The higher the SNR, the less obtrusive the noise is.

$$SNR = \frac{T}{\sigma_T} \quad (2)$$

The CNR was calculated as:

$$CNR = \frac{T-B}{\sqrt{\sigma_T^2+\sigma_B^2}} \quad (3)$$

where T and B are the average activity concentrations measured in the target and background region in the reconstructed image, respectively. $\sigma_{T,B}^2$ are the variances of these activities [5]. To quantify these values, a volume of interest (VOI) was placed around the centroid of each lesion, and within the soft tissue,

lung and liver regions of the mean and standard deviation images.

The CNR refers to the ability of the PET to distinguish between various contrasts in an acquired image and the inherent noise in the image.

The mean signal recovery of SNR and CNR were evaluated as a function of the lesion size and the lesion activity uptake, using (2) and (3).

III. RESULTS

A. *Motion Blurring versus Spatial Resolution*

A "best case scenario" images are presented in Fig. 3. and Fig. 4., from a static and dynamic simulated data.

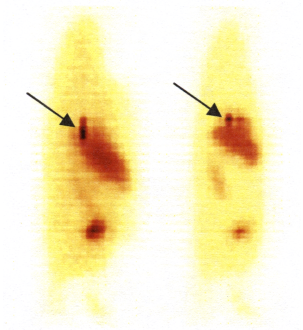

Fig. 3. Sagital slices, of the reconstructed MOBY phantom, for a dynamic acquisition (left) and a static acquisition (right), with a lung lesion of 0.75 mm diameter and an FDG uptake of 0.03 μCi.

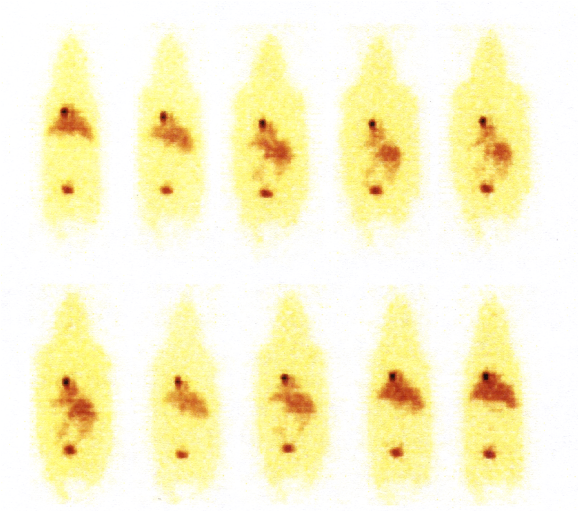

Fig. 4. Coronal slices of the MOBY phantom corresponding to the simulation of a "stress" condition breathing motion including a lung motion lesion of 1.5 mm diameter and an FDG uptake of 1.35 μCi. The coronal slices representing one respiratory cycle for an FDG exam at the last time frame. The dynamic 3D emission assumed an event collection during 900 s, where 5.65×10^9 particles were generated.

GATE and MOBY are able to provide practical phantom projection data and lung voxelized phantom respectively. From Fig. 3. and Fig. 4. differences between the non gated data set (static simulation) and the gated data set (dynamic simulation) can be seen. The extent of respiratory motion is evident between the 1st and the 10th frames in Fig. 4. The coronal slices clearly shown the realistic motion of the various structures present in the thorax and upper abdomen due to the lungs expanding and contraction for the non normal tidal breathing configuration.

From visual inspection of these figures, in the static image the lesion is clearly shown, keeping its spherical shape, and for the dynamic image, the lesion appears blurred and elongated as a consequence of the breathing movement. Consequently, respiratory motion may preclude the detection of the smallest lung lesions.

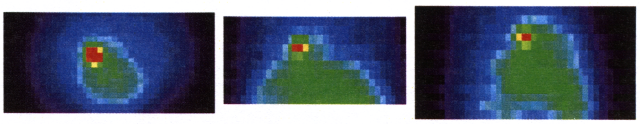

Fig. 5. Transaxial, coronal and sagital slices of the reconstructed lung lesion, in the MOBY phantom, with 2.0 mm diameter and an FDG uptake of 0.08 μCi. No motion was involved.

The motion vector defined in (1) indicates more motion blurring within transaxial plane that along axial direction. Fig. 5. clearly shows the difference of blurring along different direction. This result also indicates, due to respiratory motion, a sphere lesion can be blurred to a shape with different size in different direction in 3D space. And the extent of blurring along different direction will depends on the motion vector at the spot of the lung.

Fig. 6. shows the axial resolution, of a lesion with 0.75 mm diameter for static and dynamic acquisitions, as a function of different FDG uptakes. It demonstrates that the blurring effect is lower for static acquisitions. It also demonstrates when the FDG uptake increases the blurring increases for static acquisitions and decreases in dynamic acquisitions.

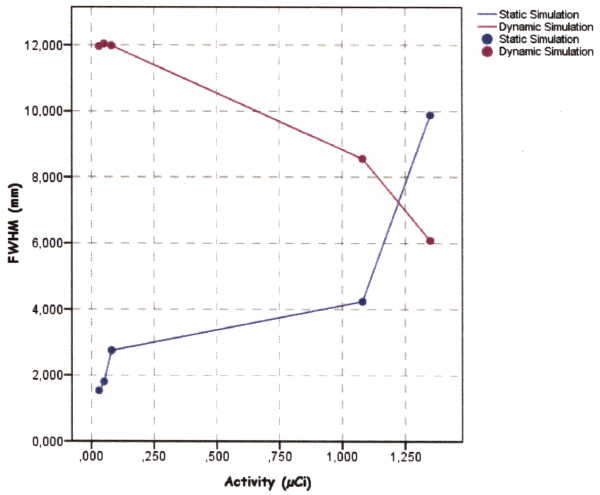

Fig. 6. FWHM of the line spread function through the lesion centroid as a function of the FDG activity defined for static and dynamic acquisitions schemes.

B. SNR and CNR

In general, the "quality" of an image can be described (quantitatively) by its SNR. The SNR directly affects diagnostic and quantitative accuracy. The SNR describes the relative "strength" of the desired information and the noise (e.g. due to the statistics of radioactive decay) in the image. The higher the SNR, the less obtrusive the noise is. The SNR is as lower as higher is the activity concentration, and is as higher as higher is the lesion diameter (Fig. 7.).

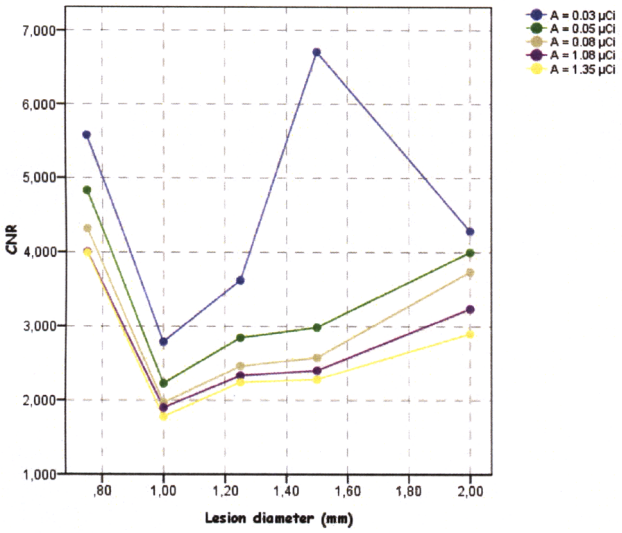

Fig. 7. SNR of the 0.03 µCi, 0.05 µCi, 0.08 µCi, 1.08 µCi and 1.35 µCi FDG uptakes for the spherical lesions as a function of the lesion diameter. Results obtained for the static simulations.

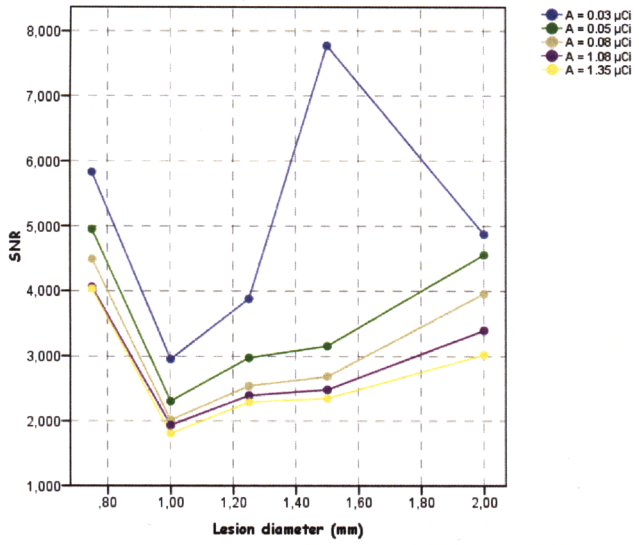

Fig. 8. CNR of the 0.03 µCi, 0.05 µCi, 0.08 µCi, 1.08 µCi and 1.35 µCi FDG uptakes for the spherical lesions as a function of the lesion diameter. Results obtained for the static simulations.

Concerning the lesion detectability (CNR), when the size of a lesion is substantially larger than the limiting spatial resolution noise can influence detectability, especially if the lesion has low contrast. The CNR is displayed in Fig. 8. as a function of the lesion diameter, and for different activity uptakes. Overall, CNR recovery improves most significantly as lesion contrast decreases and lesion size decreases. Although, the Fig. 8. shows an improvement in CNR recovery as the lesion diameter increases. This is most likely due to the fact that motion has less of an effect on the CNR for larger lesions compared to smaller lesions.

In both figures (Fig. 7 and Fig. 8.) the CNR values for the 0.75 mm lung lesion diameter are plotted but the lesion is not clearly visible, mainly for low activity contrast, and thus statistics could not be accurately measured.

Fig. 9. illustrate the relation between contrast and activity concentration, Target to Background Ratio (TBR), as a function of the lesion diameter. The higher the contrast the higher is the detectability.

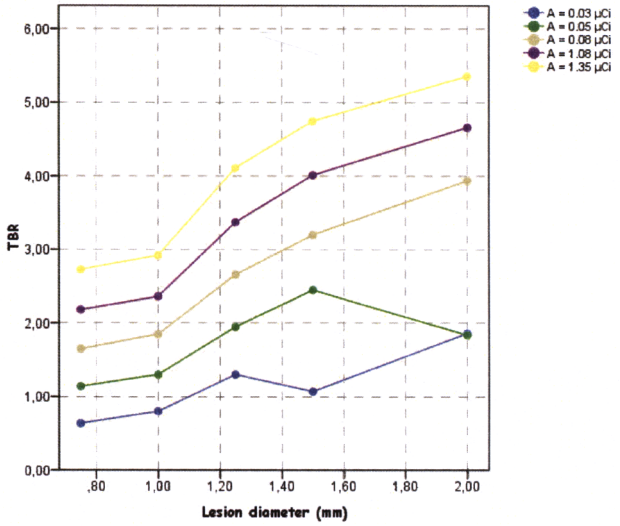

Fig. 9. TBR of the 0.03 µCi, 0.05 µCi, 0.08 µCi, 1.08 µCi and 1.35 µCi FDG uptakes for the spherical lesions as a function of the lesion diameter. Results obtained for the static simulations.

The dynamic simulations results in larger overestimations of SNR and CNR due to poor counting statistics and high image noise. This effect is more significant as the lesion diameter increases and the lesion activity concentration decreases, as it is illustrated by Fig. 10. and Fig. 11..

As discussed before, the values for the 0.75 mm lung lesion diameter for static and dynamic acquisitions are quantitatively changed due to the lesion blending into the liver.

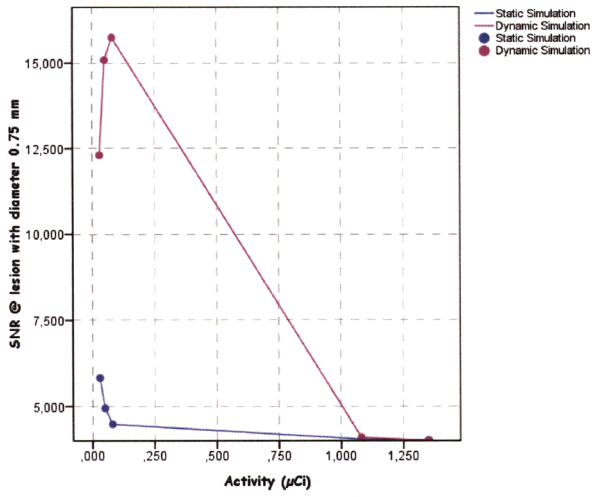

Fig. 10. SNR of a set of dynamic and static acquisitions for a lung lesion with 0.75 mm diameter as a function of the FDG activity concentration.

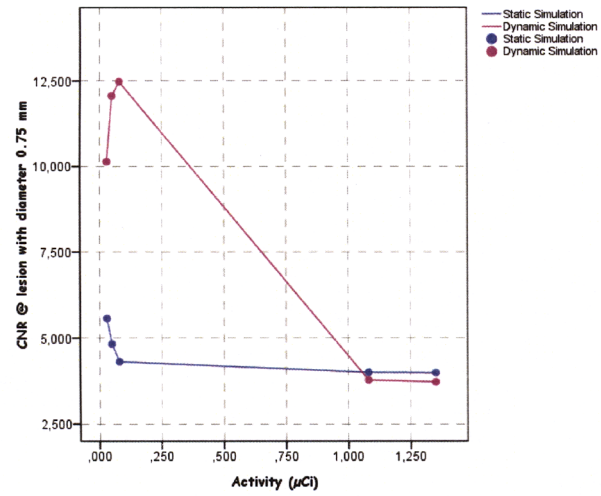

Fig. 11. CNR of a set of dynamic and static acquisitions for a lung lesion with 0.75 mm diameter as a function of the FDG activity concentration.

IV. CONCLUSIONS & PERSPECTIVES

The location and detection of lesions in thoracic and abdominal mouse imaging can be affected by the respiratory motion due to displacement of the organs during the normal breathing. This effect should be taken into account when searching lesions and quantifying tumor tracer uptake in highly deforming structures such as the lungs.

The FHWMs of reconstructed lesion images were determined along the direction of movement due to respiratory motion for static and dynamic acquisitions. The results demonstrate how the respiratory motion would affect the blurring of a lung lesion along the direction of movement.

As expected, CNR recovery improves for static acquisitions. The static images have a slightly greater CNR recovery compared to the dynamic images, which is due to the loss of resolution in the motion images. CNR recovery also improves as lesion size increases and lesion contrast decreases.

The results illustrates that the SNR deteriorate for gated data. Concerning the static acquisitions we found better SNR for lower FDG uptakes and higher lesion sizes.

This study gives an approach to evaluate the respiratory motion effect in the quantification of microPET images. A complete evaluation should also consider the other dynamic FDG simulations (gated MOBY data set) that need to be compared against the complete set of static (non-gated MOBY data set) analysis already presented in this paper.

For image reconstruction, we have used the OSEM algorithm with fixed parameters (16 subsets and 4 iterations) which are normally used in clinical standard protocol. However, there are several other image reconstruction algorithms and parameters including smoothing filters, cut-off frequency, and the number of subsets and iterations that could affect the results, but have not been addressed in this study. Further studies are required to investigate the effect of these parameters on signal and volume recovery.

Background activity is unavoidable and it causes significant noise and contrast loss in PET images [6]. The effect of background activity concentration will be analyzed in the next phases of this research.

As discussed before, respiratory motion leads to reduced contrast and quantitative accuracy in terms of recovered contrast activity concentration and functional volumes. Several methodologies proposed for reducing the effects of respiratory motion has been based on the development of respiratory gated acquisitions [7], [8]. But, in general, 4D PET images have low counting statistics and high image noise compared to static 3D PET images. Since the same number of coincidences events in 3D PET is divided into many different respiratory phase bins or time frames, the number of coincidence events per image bin is considerably reduced. This leads to higher image noise in 4D PET images. Therefore, there is a tradeoff between image noise and temporal resolution. Long duration time per frame gives low noise but blurred images resulting from the loss of temporal resolution [6]. In order to determine the effect of the number of gating bins on image noise and temporal resolution, sets of 4D simulations will be performed for the MOBY phantom following the same line of reasoning for these studies.

Therefore, there is still the need for a method which takes into account the effect of respiratory motion without, at the same time, affecting the quantification analysis on the reconstructed images. For that reason, this work is being complemented by accessing the impact of such motion in the quantification analysis using a dynamic VOI, placed around the centroid of each lesion, for the 4D images studies.

REFERENCES

[1] Jan, S. et al., "GATE: a simulation toolkit for PET and SPECT," *Physics in Medicine and Biology*, vol. 49, no.19. pp. 4543-4561, August 2004.

[2] Tai, Y. et al., "Performance Evaluation of the microPET FOCUS: A Third-Generation microPET Scanner Dedicated to Animal Imaging," *Journal of Nuclear Medicine*, vol. 46, pp. 455-463, March 2005.

[3] Jan, S. et al., "Monte Carlo simulation of the microPET FOCUS system for small rodents imaging applications," *IEEE Nuclear Science Symposium Conference Record*, vol. 3, pp.1653-1657, October 2005.

[4] William P. Segars, Benjamin M. W. Tsui, Eric C. Frey, G. Allan Johnson and Stuart S. Berr, "Development of a 4-D Digital Mouse Phantom for Molecular Imaging Research," *Molecular Imaging and Biology*, vol. 6, no. 3, pp. 149-159, May-June 2004.

[5] C. Lartizien, P. Kinahan, and C. Comtat, "A Lesion Detection Observer Study Comparing 2-Dimensional Versus Fully 3-Dimensional Whole-Body PET Imaging Protocols," *Journal of Nuclear Medicine*, vol. 45, pp. 714-723, April 2004.

[6] Sang-June Park et al., "Evaluation of the combined effects of target size, respiratory motion and background activity on 3D and 4DPET/CT images," *Physics in Medicine and Biology*, vol. 53, pp. 3661-3679, June 2008.

[7] Sadek A. Nehmeh et al., "Effect of Respiratory Gating on Quantifying PET Images of Lung Cancer," *The Journal of Nuclear Medicine*, vol. 43, no.7, pp. 876-881, July 2002.

[8] D. Visvikis, F. Lamare, P. Bruyant, N. Boussion and C. Cheze Le Rest, "Respiratory motion in positron emission tomography for oncology applications: Problems and Solutions," *Nuclear Instruments and Methods in Physics Research A*, vol. 569, pp. 453-457, October 2006.